

Electronic Supplementary Information

Symmetry-Breaking Charge Separation in Nitrogen-Bridged Naphthalene Monoimide Dimer

*Xinmiao Niu,^{a,b,c} Keita Tajima,^d Jie Kong,^{b,c} Min Tao^{b,c} Norihito Fukui,^{*d} Zhuoran Kuang,^{*,a} Hiroshi Shinokubo,^{*,d} Andong Xia^{*,a,c}*

^a State Key Laboratory of Information Photonic and Optical Communications, School of Science, Beijing University of Posts and Telecommunications (BUPT), Beijing 100176, People's Republic of China

^b Beijing National Laboratory for Molecular Sciences (BNLMS), Key laboratory of Photochemistry, Institute of Chemistry, Chinese Academy of Sciences, Beijing 100190, People's Republic of China

^c University of Chinese Academy of Sciences, Beijing 100049, People's Republic of China

^d Department of Molecular and Macromolecular Chemistry, Graduate School of Engineering, Nagoya University, Furo-cho, Chikusa-ku, Nagoya, Aichi 464-8603, Japan

Corresponding Author

* Andong Xia, E-mail: andong@iccas.ac.cn

* Hiroshi Shinokubo, E-mail: hshino@chembio.nagoya-u.ac.jp

* Zhuoran Kuang, Email: kuang@bupt.edu.cn

* Norihito Fukui, Email: fukui@chembio.nagoya-u.ac.jp

Table of Contents

S1. Fluorescence lifetime measurements.

S2. DFT/TD-DFT optimized geometries of *bis*-ANI.

S3. Electrochemical measurements and the radical cation and anion spectra of ANI and NI.

S4. Fitting results of femtosecond transient spectra of ANI and *bis*-ANI in HEX.

S5. Kinetics of femtosecond transient absorption spectra of ANI and *bis*-ANI at selected wavelengths.

S1. Fluorescence lifetime measurements.

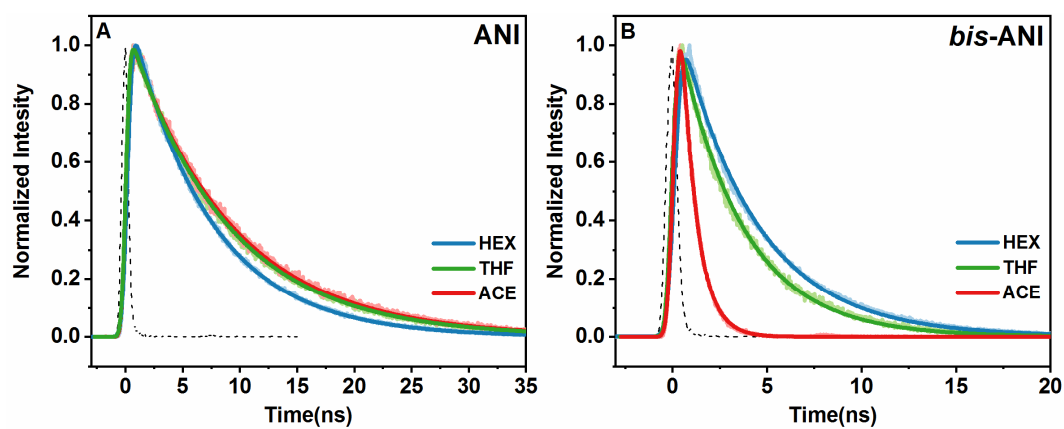


Figure S1. Fluorescence lifetimes of (A) ANI and (B) *bis*-ANI. Fitting results are also included.

S2. DFT/TD-DFT optimized geometries of *bis*-ANI.

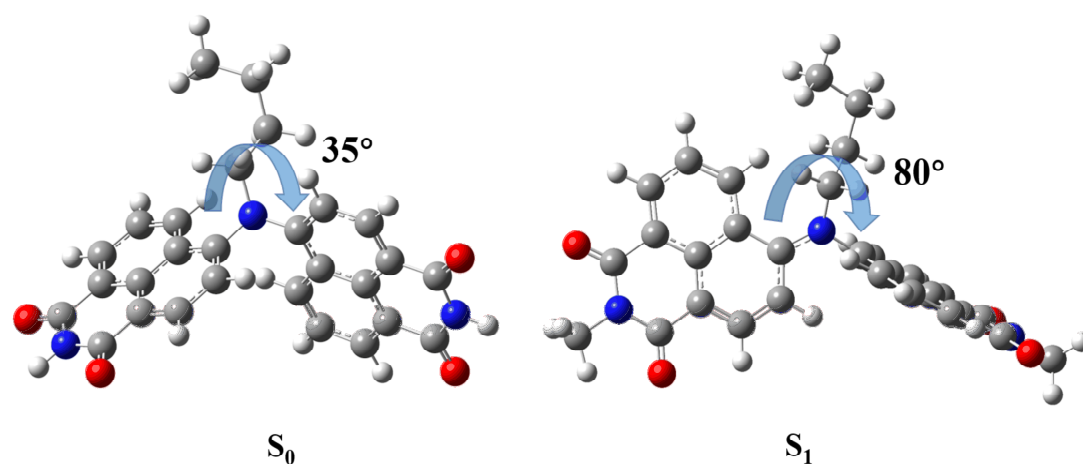


Figure S2. The optimized ground state (S_0) and excited state (S_1) geometries of *bis*-ANI.

Table S1. Electronic excitation properties of ANI and *bis*-ANI at optimized S_0 and S_1 geometries.

	ANI		<i>Bis</i> -ANI	
	optimized S_0 geometry	optimized S_1 geometry	optimized S_0 geometry	optimized S_1 geometry
E (eV)	3.67 eV	3.14 eV	3.54 eV	2.76 eV
oscillator strength	0.33	0.28	0.48	0.10
main orbital contribution	H→L 97%	H→L 98%	H→L 82%	H→L 92%

S3. Electrochemical measurements and the radical cation and anion spectra of ANI and NI.

To calculate the Gibbs free energy and prove the formation of new bands in the fs-TA of *bis*-ANI in THF and ACE, we perform the Cyclic voltammetry and spectroelectrochemical measurements of ANI and NI.

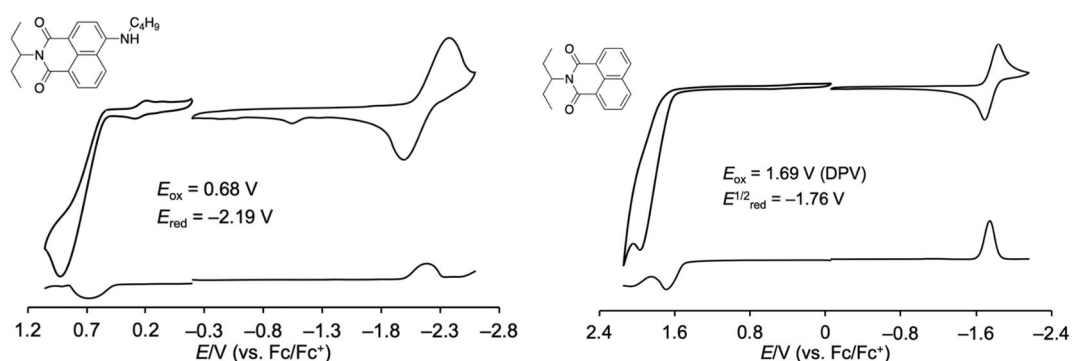


Figure S3. Cyclic voltammograms and differential pulse voltammograms (DPVs) of ANI and NI. Redox potentials were measured by cyclic voltammetry in anhydrous THF for ANI and CH₃CN for NI using 0.1 M [Bu₄N][PF₆] as the supporting electrolyte and Ag/AgNO₃ as the reference electrode. The ferrocene/ferrocenium ion couple was used as an external reference.

We also conducted spectroelectrochemical measurements of NI and ANI (Figures S4-5) for identifying the observed new species of fs-TA. The electrochemical oxidation of NI and ANI generated no apparent absorption peak in the range of 400–750 nm, which nicely accords with the fact that the absorption due to the radical cation moiety cannot be observed in the measured window of fs-TA. The electrochemical reduction of NI afforded new absorption peaks at 415 and 488 nm while that of ANI generated new absorption bands around 540 nm. Based on these experiments, we can conclude that the SBCS state of *bis*-ANI mainly contains NI^{•-} as the radical anion unit.

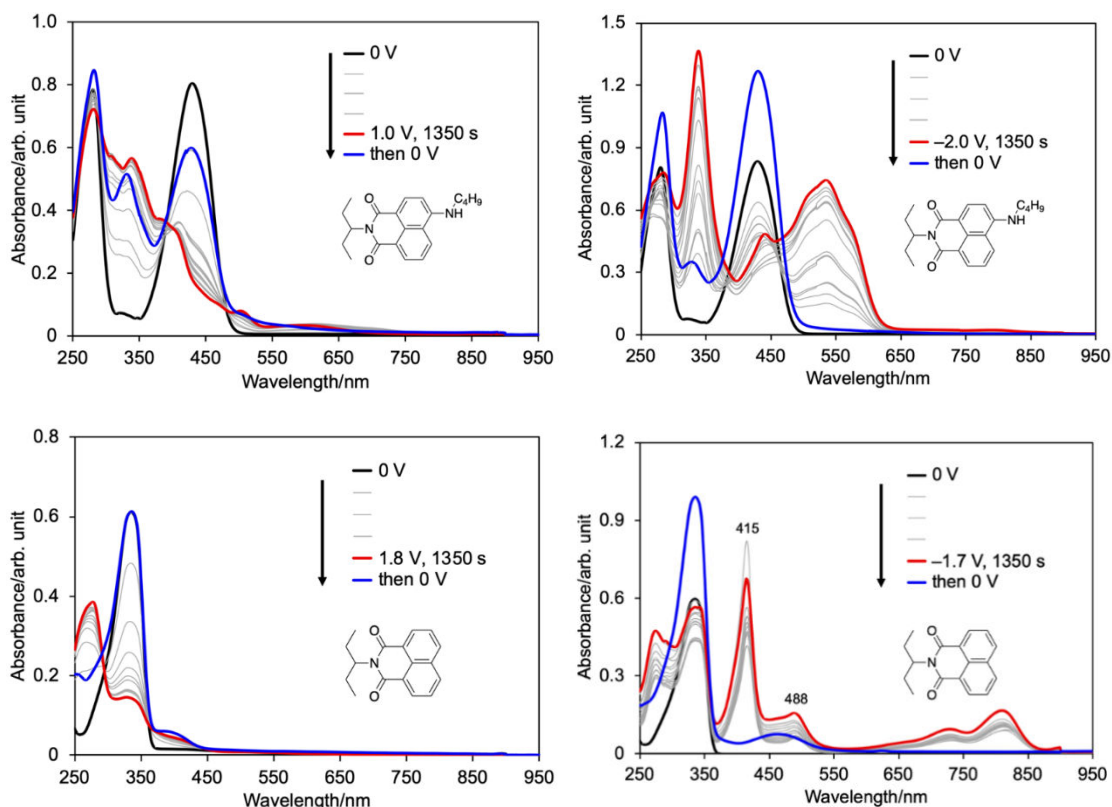


Figure S4. Spectral change in the absorption of ANI and NI during electrochemical redox process.

Table S2. Gibbs free energy of charge separation of *bis*-ANI.

	solvent	$E_{\text{ox}}(\text{V})^{\text{a}}$	$E_{\text{red}}(\text{V})^{\text{a}}$	$E_{\text{ox}} - E_{\text{red}}$	$E_{0,0}(\text{V})$	$\Delta G_{\text{CS}}(\text{eV})$
$E_{\text{ox}}(\text{NI}) - E_{\text{red}}(\text{NI})$	HEX	1.69	-1.76	3.45 V	2.78	1.10
	THF	1.69	-1.76	3.45 V	2.59	0.91
	ACE	1.69	-1.76	3.45 V	2.57	0.62
$E_{\text{ox}}(\text{NI}) - E_{\text{red}}(\text{ANI})$	HEX	1.69	-2.19	3.88 V	2.78	1.50
	THF	1.69	-2.19	3.88 V	2.59	1.35
	ACE	1.69	-2.19	3.88 V	2.57	0.92
$E_{\text{ox}}(\text{ANI}) - E_{\text{red}}(\text{NI})$	HEX	0.68	-1.76	2.44 V	2.78	0.09
	THF	0.68	-1.76	2.44 V	2.59	-0.10
	ACE	0.68	-1.76	2.44 V	2.57	-0.39

^a The data are taken from Figure S3;

In the latter two terms, $\frac{e^2}{4\pi\epsilon_0\epsilon_s r_{DA}}$ and $\frac{e^2}{8\pi\epsilon_0} \left(\frac{1}{r_D} + \frac{1}{r_A} \right) \left(\frac{1}{\epsilon_{\text{ref}}} - \frac{1}{\epsilon_s} \right)$, ϵ_s is the static dielectric constant of the solvent; $\epsilon_0 (= 5.526 \times 10^{-3} \text{ eV}^{-1} \text{ \AA}^{-1})$ is the permittivity of free space¹; ϵ_{ref} is the dielectric constant of the reference solvent (dichloromethane: 8.93) used in electrochemistry.

S4. Fitting results of femtosecond transient spectra of ANI and *bis*-ANI in HEX.

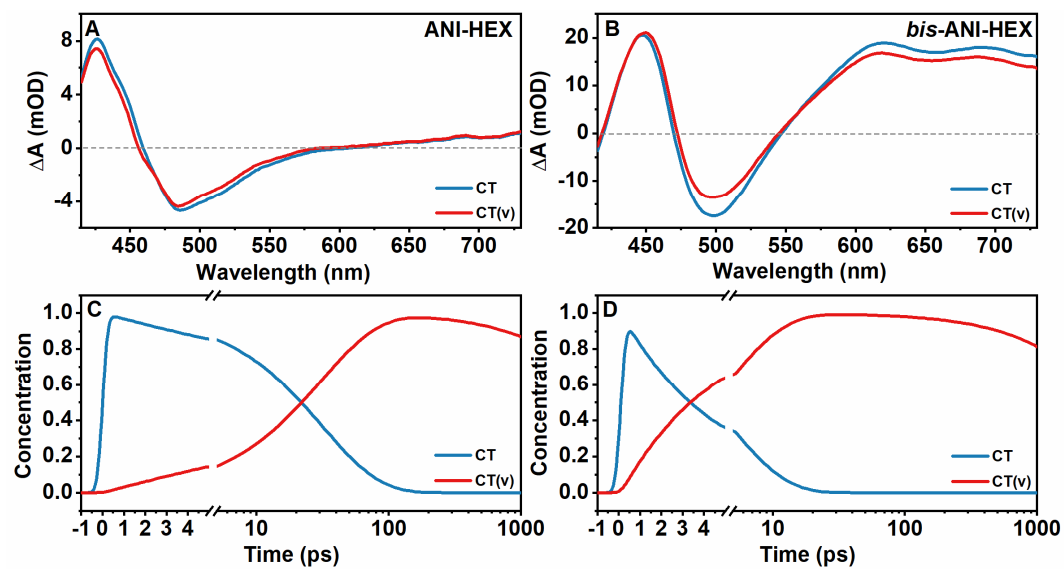


Figure S5. EADS from global analysis of ANI (A) and *bis*-ANI (B) in HEX; Concentration evolution of transient species of ANI (C) and *bis*-ANI (D) in HEX.

S5. Kinetics of femtosecond transient absorption spectra of ANI and *bis*-ANI at selected wavelengths.

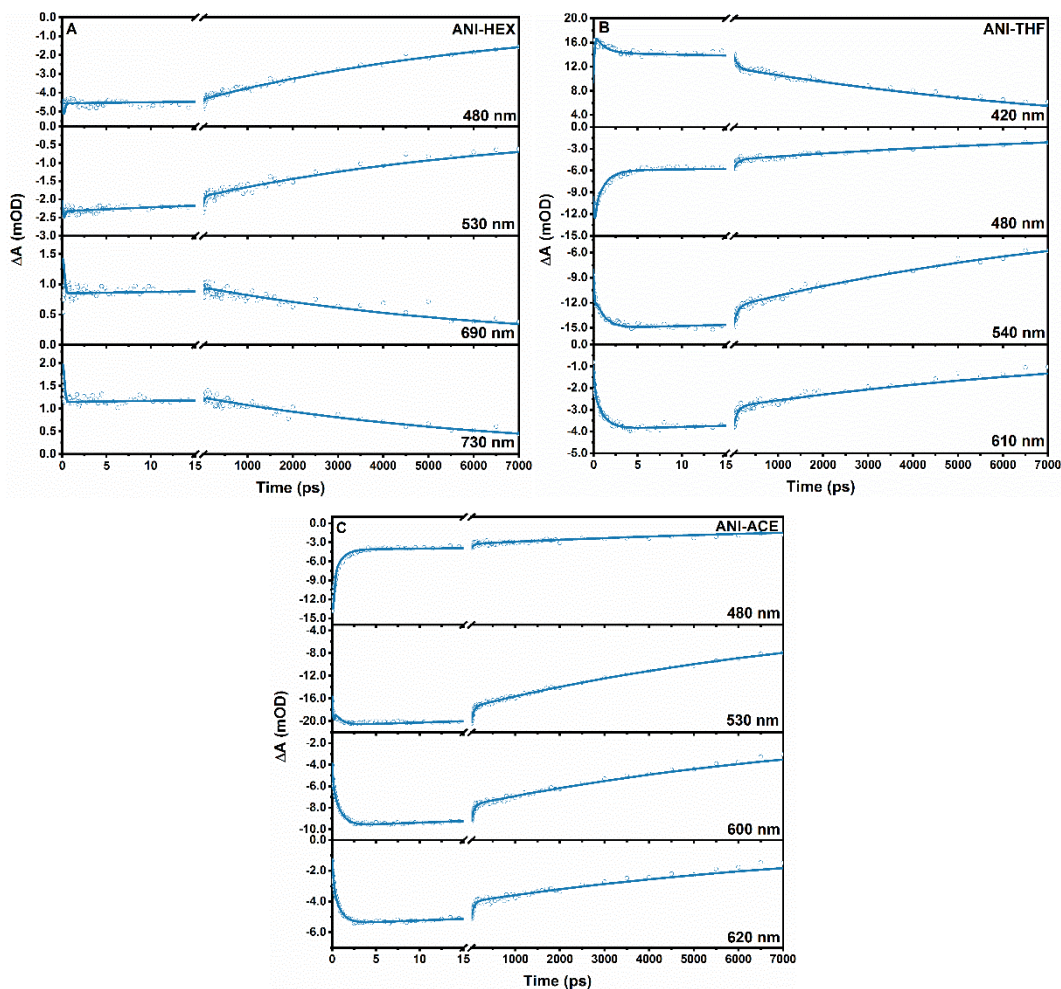


Figure S6. Kinetics of femtosecond transient absorption spectra of ANI in HEX, THF and ACE at selected wavelengths are plotted (dot) together with global fitting curves (line) of all collected time traces for showing the fitting quality. For ANI in HEX, 480, 530, 690 and 730 nm wavelengths are selected (A), for ANI in THF, 420, 480, 540 and 610 nm wavelengths are selected (B), and for ANI in ACE, 480, 530, 600 and 620 nm wavelengths are selected (C), for showing the fitting quality.

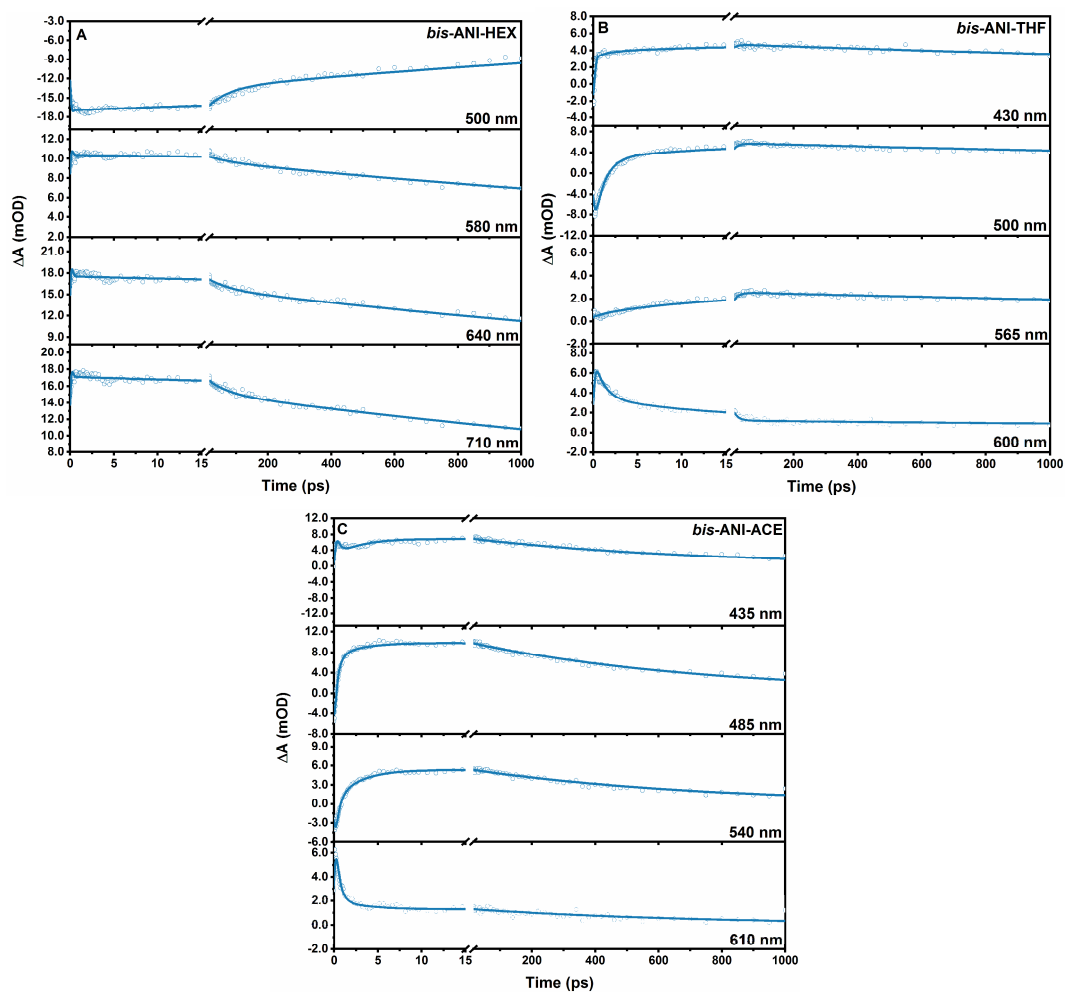


Figure S7. Kinetics of femtosecond transient absorption spectra of *bis*-ANI in HEX, THF and ACE at selected wavelengths are plotted (dot) together with global fitting curves (line) of all collected time traces for showing the fitting quality. For *bis*-ANI in HEX, 440, 560, 660 and 740 nm wavelengths are selected (a), for *bis*-ANI in THF, 430, 550, 650 and 720 nm wavelengths are selected (b), for *bis*-ANI in ACE, 500, 595, 640 and 725 nm wavelengths are selected (c), for showing the fitting quality.

Reference

1. M. L. Horng, J. A. Gardecki, A. Papazyan and M. Maroncelli, *J. Phys. Chem.*, 1995, **99**, 17311-17337.